Hyperparametric Oscillation via Bound States in the Continuum

Hyperparametric Oscillation via Bound States in the Continuum

Fuchuan Lei, Zhichao Ye, Krishna Twayana, Yan Gao, Marcello Girardi, Óskar B. Helgason, Ping Zhao, and Victor Torres-Company*

Department of Microtechnology and Nanoscience, Chalmers University of Technology SE-41296 Gothenburg, Sweden

(Received 7 June 2022; accepted 4 January 2023; published 28 February 2023)

Optical hyperparametric oscillation based on the third-order nonlinearity is one of the most significant mechanisms to generate coherent electromagnetic radiation and produce quantum states of light. Advances in dispersion-engineered high-Q microresonators allow for generating signal waves far from the pump and decrease the oscillation power threshold to submilliwatt levels. However, the pump-to-signal conversion efficiency and absolute signal power are low, fundamentally limited by parasitic mode competition and attainable cavity intrinsic Q to coupling Q ratio, i.e., Q_i/Q_c. Here, we use Friedrich-Wintgen bound states in the continuum (BICs) to overcome the physical challenges in an integrated microresonator-waveguide system. As a result, on-chip coherent hyperparametric oscillation is generated in BICs with unprecedented conversion efficiency and absolute signal power. This work not only opens a path to generate high-power and efficient continuous-wave electromagnetic radiation in Kerr nonlinear media but also enhances the understanding of a microresonator-waveguide system—an elementary unit of modern photonics.

DOI: 10.1103/PhysRevLett.130.093801

Optical hyperparametric oscillation (H-OPO) emerges in a driven $\chi^{(3)}$ nonlinear cavity as a result of modulation instability (MI) that amplifies vacuum photons. Two pump photons are converted into a pair of correlated photon pairs ($2\hbar\omega_p \rightarrow \hbar\omega_s + \hbar\omega_i$) at new frequencies [Fig. 1(a)]. This elementary mechanism lies at the onset of microresonator frequency comb generation [1] and has served for generating coherent light sources [2–7] and quantum technologies [8–14]. High-Q microresonators, either in whispering gallery mode [15,16], planar [17–24], or photonic crystal cavities [25], provide means to decrease the power oscillation threshold. With dispersion engineering, broadband H-OPO has been demonstrated [26–30].

A critical metric in any parametric oscillator is the conversion efficiency, i.e., the ratio of signal power compared to the pump. This metric is first limited by mode competition among different longitudinal modes in the cavity and nondegenerate four-wave mixing [31]. The gain required to sustain H-OPO originates from MI. For a fixed dispersion, the gain's peak and bandwidth are determined by the pump power [32,33]. With high pump power, the gain can span multiple free spectral ranges (FSRs), even for extremely small cavities [34,35], as schematically illustrated in Fig. 1(b). Hence, multiple cavity modes could emit simultaneously once their losses are compensated by the gain. The newly generated frequency components could induce by themselves parametric oscillation, and degrade the coherence through nondegenerate four-wave mixing [34]. To avoid these detrimental effects, one could engineer the resonator's dispersion and pump it with moderate power [26–30,36]. Another strategy is to reduce the number of effective cavity modes, such as

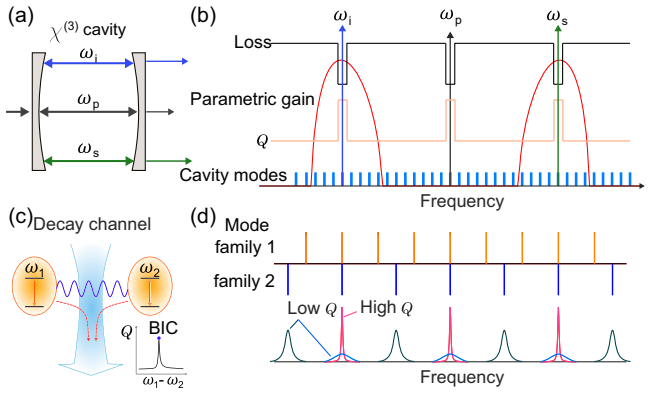

FIG. 1. Concept of H-OPO via bound states in the continuum (BICs). (a) Schematic of H-OPO. (b) Cavity quality factor (Q) management for achieving high-efficiency H-OPO. (c) Schematic illustration of the Friedrich-Wintgen BIC. Two near degenerate resonances can be dissipatively coupled if both share a common decay channel. As a result, two supermodes are formed: one is a nondecaying bound state (high Q) while the other one is an increased-decaying state (low Q). (d) Realization of (Q) engineering for cavity modes by making use of BICs in a two-mode cavity, where the high-Q mode can be achieved periodically owing to the Vernier effect.

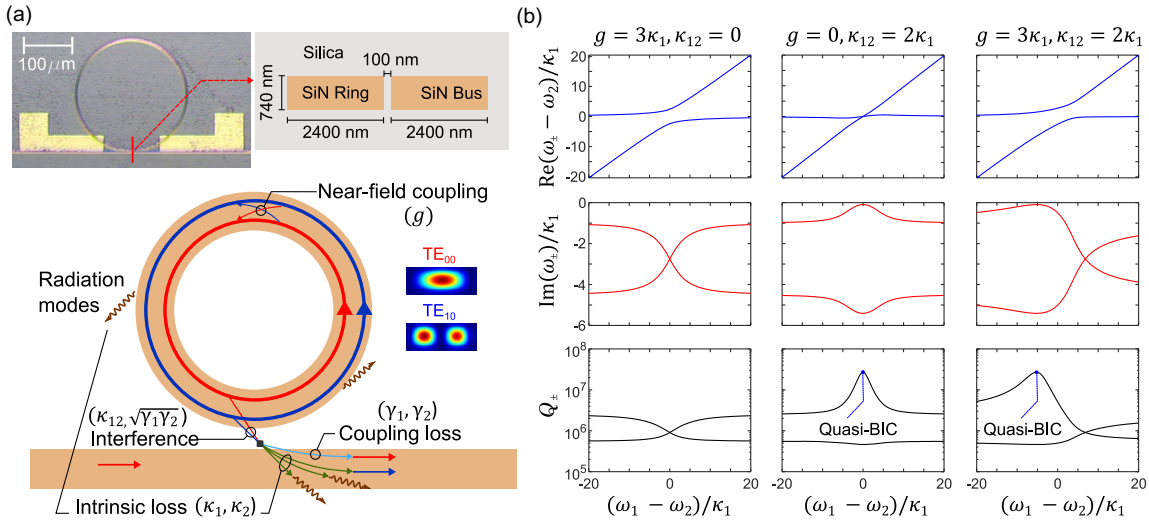

FIG. 2. BICs in a multimode microring-waveguide system. (a) Image and schematic of the system. (b) Calculated eigenfrequencies of $\mathcal{H}$ and the corresponding Q as a function of the detuning. Parameters used here: $\gamma_1 = \gamma_2 = 0$, $\kappa_2 = 4.5\kappa_1$, $\omega_1/\kappa_1 = 5 \times 10^6$.

increasing the FSR of microresonators [28,31] or suppressing undesired modes with the aid of frequency selection elements [see Fig. 1(b)], e.g., coupled cavities and gratings [37,38]. These classical techniques, being widely used for single-frequency lasers, however, cannot be directly adapted for nonlinear optics because they are usually incompatible with the stringent demand of simultaneously attaining high-Q, low-mode volume and dispersion engineering. In addition to multimode interaction, the second limiting factor of the conversion efficiency is the attainable Q_i/Q_c [26], where $Q_{i(c)}$ is the cavity intrinsic (coupling) quality factor. Realistic microresonator-coupler systems introduce a physical limit because the coupling rate ($\sim 1/Q_c$) cannot be arbitrarily high without involving additional intrinsic loss, hence, decreasing Q_i [39,40].

In this Letter, we demonstrate that the abovementioned limits can be overcome simultaneously by exploiting the concept of bound states in the continuum (BICs). As a result, high-efficiency H-OPO could be accomplished. BICs were originally proposed by von Neumann and Wigner nearly one century ago in quantum physics, and in recent years they have been extended to many other fields [41,42]. In photonics, BICs can be used to trap light and obtain high-Q modes [43–48], leading to applications such as lasing [49–51], sensing [52,53], and nonlinear optics [54–59]. Here we implement the Friedrich-Wintgen BICs in an integrated multimode microresonator-waveguide system. As schematically shown in Fig. 1(c), Friedrich-Wintgen BICs can occur as a result of destructive interference if two near degenerate resonances are dissipatively coupled through a common decay channel [60,61]. Mathematically, Friedrich-Wintgen BICs are one type of singularity in anti-parity-time symmetric systems [49,62–67]. To utilize the concept of BICs for the mode number-dependent Q factor management, we take advantage of the Vernier effect in multimode microresonators [Fig. 1(d)].

We consider an experimental system which consists of a silicon nitride (Si_3N_4) microring resonator and an adjacent bus waveguide, as shown in Fig. 2(a). Both the ring and bus waveguide support the higher-order modes TE_{10} and TE_{20} in addition to the fundamental mode TE_{00}. The TE_{20} can be ignored in practice because its Q is much lower. Unlike most widely used microring-waveguide systems, the ring-bus gap here is very small, which allows the fundamental cavity modes to couple with the other (guided and radiation) modes in the bus waveguide besides the fundamental one; see Fig. 2(a). This results in parasitic loss for the cavity mode and an encompassing reduction in Q_i and coupling ideality [40]. The role of the bus waveguide on the intrinsic property of microcavities is not sufficiently appreciated [68], but it can have a dramatic influence, especially in multimode cavities [69–71]. In particular, the parasitic loss caused by the bus waveguide can be coherently suppressed when two near resonant cavity modes exist. In this case, Friedrich-Wintgen BICs could emerge because two cavity modes are coupled with the same decay channels. The motion of two near resonant cavity modes can be described by a Schrödinger-type equation (see Supplemental Material [72]

$$i\frac{\partial}{\partial t}|\psi\rangle = \mathcal{H}|\psi\rangle + |s\rangle, \tag{1}$$

$$\mathcal{H} = \begin{pmatrix} \omega_1 & g \\ g^* & \omega_2 \end{pmatrix} - i\begin{pmatrix} \kappa_1 & \kappa_{12} \\ \kappa_{12}^* & \kappa_2 \end{pmatrix} - i\begin{pmatrix} \gamma_1 & \sqrt{\gamma_1\gamma_2} \\ \sqrt{\gamma_1\gamma_2} & \gamma_2 \end{pmatrix} \tag{2}$$

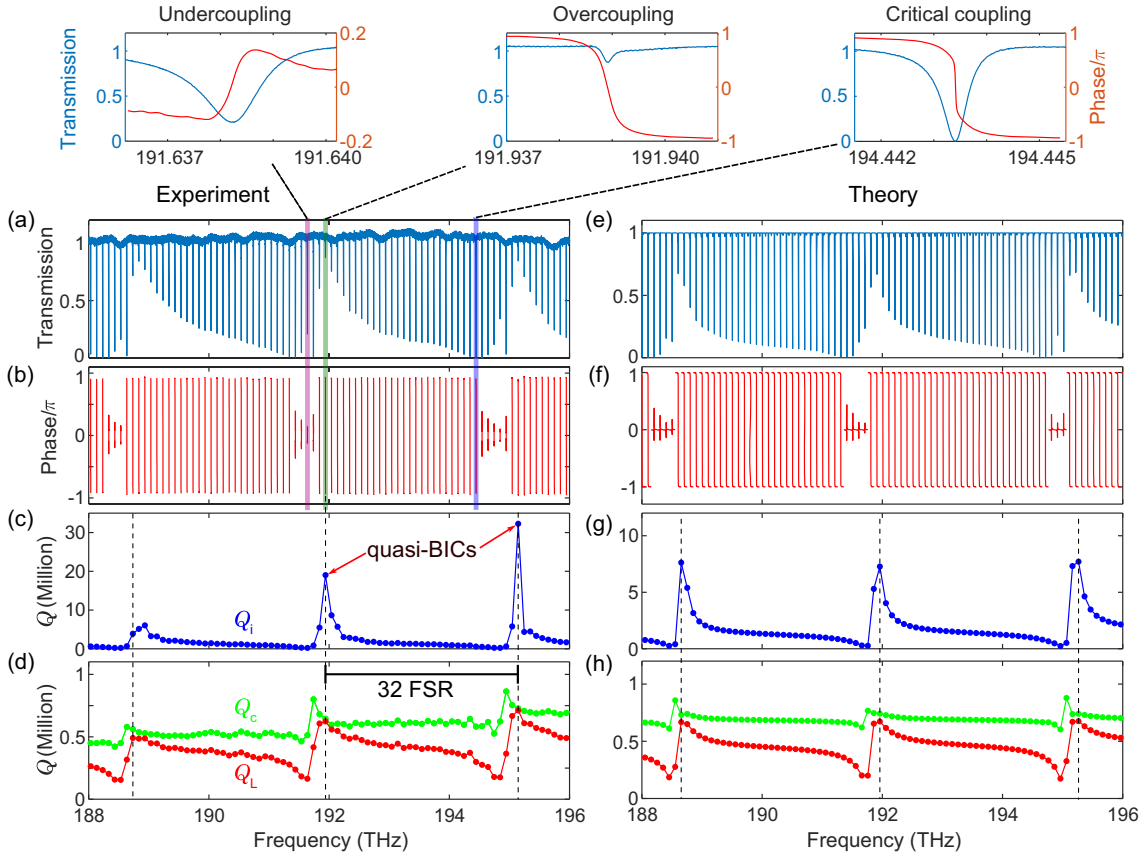

FIG. 3. Observation of BICs via spectral characterization of the system. (a) Normalized transmission scan of the microring-waveguide system. (b) Effective phase response of the system. (c) Intrinsic and (d) coupling as well as loaded Q factors for the measured resonances. Three coupling conditions: undercoupling, overcoupling, and critical coupling are enlarged in the top panel. (e)–(h) Theoretical results corresponding to the case in panels (a)–(d).

with $|\psi\rangle = [a_1, a_2]^T$, $|s\rangle = [\sqrt{2\gamma_1}, \sqrt{2\gamma_2}]^T s_{\text{in}}$, where the $a_{1(2)}$ are the complex amplitudes of the TE_{00} and TE_{10} cavity modes. In the first term of $\mathcal{H}$, $\omega_{1(2)}$ are the resonant frequencies in the uncoupled system, and g is the scattering-induced direct coupling coefficient between the two modes. The second term of $\mathcal{H}$ is non-Hermitian, where $\kappa_{1(2)}$ stand for the decay rates caused by intrinsic loss including material absorption, radiation loss, and bus-waveguide-induced parasitic loss. κ_{12} denotes the via-the-continuum coupling term since the two cavity modes share the same decay channels. This is the critical parameter for achieving high-Q_i BIC modes. We note that the value of κ_{12} is restricted to $|\kappa_{12}| < \sqrt{\kappa_1\kappa_2}$ as not all decaying terms can be canceled by perfect destructive interference; i.e., only quasi-BICs can be attained. The third term of $\mathcal{H}$ describes the two cavity modes coupling to the fundamental mode of the bus waveguide at rates $\gamma_{1(2)}$. The term $\sqrt{\gamma_1\gamma_2}$ plays a role similar to κ_{12} to generate BICs, but it acts on Q_c instead of Q_i [44]. It is worth noting that Q_i and Q_c play the same role in $\mathcal{H}$, but their impact on the light coupling and thus the efficiency of the nonlinear optics process is quite different.

BICs can be obtained from the eigenvalues ($\omega_\pm$) of $\mathcal{H}$. The real and imaginary parts of the eigenvalues stand for the resonant frequencies and decay rates of two eigenmodes formed by the superposition of the original cavity modes. The quality factors of the two eigenmodes can be calculated by $Q_\pm = |\text{Re}(\omega_\pm)/2\text{Im}(\omega_\pm)|$. Because of coupling, both of the resonant frequencies and decay rates vary with the detuning ($\omega_1 - \omega_2$). To illustrate that Q_i can be tailored as a result of BICs, we assume $\gamma_{1(2)} = 0$ and plot the complex frequencies as a function of the detuning; see Fig. 2(b). It is shown that the scattering-induced near field direct coupling (g) and via-the-continuum indirect coupling (κ_{12}) lead to distinct effects on the eigenvalues. The former leads to the real parts of eigenvalues being avoided and imaginary parts crossed, while the latter gives rise to the opposite effect. Moreover, when only one eigenvalue becomes near purely real, a quasi-BIC is formed at the expense of the other eigenvalue becoming more lossy (its imaginary part increases). In a realistic system, both direct coupling and indirect coupling exist; thus, the interference at the coupling region is determined by both. In this scenario, quasi-BICs can still be obtained but, surprisingly at a nonzero detuning, while the Q's also exhibit asymmetric dependence on the

detuning. These aspects will be demonstrated in the following experiment.

The bus waveguide features a tapered structure at both ends to ensure only TE_{00} can be excited and collected. The measured normalized transmission spectrum of the system is shown in Fig. 3(a). Unlike the conventional transmission spectrum of a microring-waveguide system, a doubly periodic pattern shows up, given by the nominal FSR of the fundamental mode and a periodic deletion the transmission resonance that arises from the interaction between between TE_{00} and TE_{10} mode families. The period is 32 FSRs of the TE_{00} mode, which matches the Vernier frequency corresponding to the walk-off between group indices (see Supplemental Material [72]).

Although two transverse modes families are involved, it is noted that only a single clear resonance dip can be observed within each FSR dominated by TE_{00} family modes. This can be interpreted as the low-Q_i eigenmodes being extremely undercoupled. Therefore, the transmission spectrum and phase response can be approximately considered as the consequence of single high-Q_i eigenmodes. The measured transmittance and phase allow us to distinguish unambiguously Q_i and Q_c; see Fig. 3 and Fig. S2 in the Supplemental Material [72].

Following the transmission spectrum, both Q_i and Q_c feature periodic patterns but with slightly shifted frequency dependence, which could be explained as the intrinsic loss and coupling loss of cavity modes correspond to different decay channels. As discussed above, due to the coexistence of direct and indirect coupling, both Q_i and Q_c as well as the transmission spectrum exhibit a Fano-like frequency dependence. The asymmetric Q distribution with respect to the pump mode further reduces the risk of mode competition in H-OPO as demonstrated in the following section. In addition to suppressing mode competition, another advantage of engineering Q_i is that the modes with highest Q_L are strongly overcoupled (top panel of Fig. 3). This counterintuitive phenomenon is especially important for achieving high-efficiency nonlinear optics phenomena, and H-OPO in particular.

The above theoretical model only considers the interaction between a pair of near resonant modes. To better describe the realistic system over a wider spectral range, we generalize the above model to four interacting modes (see Supplemental Material [72]) by including the effect that one mode from the TE_{00} family could couple to more than one mode from the TE_{10} family simultaneously and vice versa; see Figs. 3(e)–3(h). The good match between theory and experiment suggests our model captures the main underlying physics of the system.

To generate H-OPO, anomalous dispersion is required. We found the supermode's dispersion is dominated by the TE_{00} mode with mode-interaction-induced distortion (see Supplemental Material [72]). To pump this device, we use a laser located at 1561.9 nm after being amplified by an erbium-doped fiber amplifier. The on-chip pump power threshold of this H-OPO is ~60 mW, and the highest conversion efficiency is attained at 200 mW. To couple pump into resonance, we decrease the laser's frequency gradually. With more pump power coupled into the microresonator, a pair of signal and idler waves are generated, exactly located at the quasi-BIC locations; see Fig. 4(a). With further decreasing the pump frequency, the power of the signal and idler increases linearly before reaching saturation [see Fig. 4(b)]. The maximum conversion efficiency $\eta_s = (P_s + P_i)/P_0 = 68\%$ corresponding to ~70 mW on-chip signal power. The value could be further improved if the undesired BICs (i.e., BICs modes excluding pump, signal, and idler modes) and the resultant cascaded four-wave mixing were suppressed (see Supplemental Material [72]), for example, by coupling with an auxiliary cavity [77]. By further reducing the detuning, the conversion efficiency decreases suddenly as a result of the birth of new lines, indicating the low-Q modes can still be activated at high pump power. The advantage of BICs can be clearly shown if we pump another sample, which has the same geometric parameters except for a 50 nm larger ring-bus gap. Hence, it does not feature quasiperiod Q response, and the highest conversion efficiency is limited to $< 15\%$ due to mode competition.

To conclude, we have implemented BICs in an integrated Kerr nonlinear microring resonator featuring a high-contrast quasiperiodic response in quality factor. By exploring

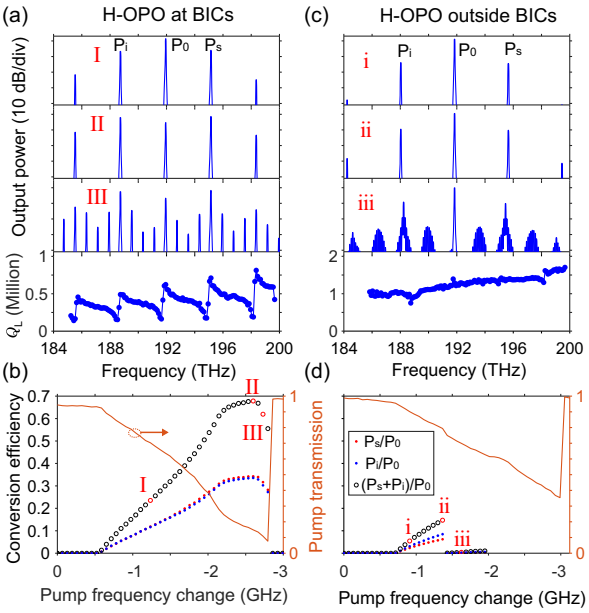

FIG. 4. Experimental demonstration of H-OPO in microresonators at and outside BICs. (a) Measured optical spectra at different pump-cavity detunings. As a reference, frequency-dependent loaded Q (Q_L) is plotted at the bottom. (b) Calculated conversion efficiency and pump transmission as a function of the pump frequency. (c),(d) same as (a),(b) except for pumping another sample.

waveguide-assisted dissipative mode coupling in microring-waveguide system, we have generalized the spectral response and demonstrated the feasibility of boosting Q_i in high-Q microresonators. Such a simple system not only enables the unwanted modes to be suppressed, but it also allows us to obtain strong overcoupling without sacrificing Q_i for desired modes. The Q_i can in fact be higher than in standard single-mode systems, resulting in unprecedented efficiency in H-OPO and high-power signal and idler waves. Besides H-OPO, the possibility to engineer the spectral response of the intrinsic quality factor of high-Q microresonators can be useful for other power-efficient nonlinear optics scenarios, and the strong overcoupling (high Q_i/Q_c) could especially facilitate the generation of squeezed or entangled states of light [8,77–80].

The raw data for this work can be accessed from Ref. [81].

The devices demonstrated in this work were fabricated at Myfab Chalmers. This work was supported by European Research Council (CoG GA 771410) and Vetenskapsrådet (2020-00453).

*torresv@chalmers.se

[1] P. Del'Haye, A. Schliesser, O. Arcizet, T. Wilken, R. Holzwarth, and T. J. Kippenberg, Nature (London) **450**, 1214 (2007).
[2] T. J. Kippenberg, S. M. Spillane, and K. J. Vahala, Phys. Rev. Lett. **93**, 083904 (2004).
[3] A. A. Savchenkov, A. B. Matsko, D. Strekalov, M. Mohageg, V. S. Ilchenko, and L. Maleki, Phys. Rev. Lett. **93**, 243905 (2004).
[4] C. Y. Wang, T. Herr, P. Del'Haye, A. Schliesser, J. Hofer, R. Holzwarth, T. W. Hänsch, N. Picqué, and T. J. Kippenberg, Nat. Commun. **4**, 1345 (2013).
[5] Y. Yang, X. Jiang, S. Kasumie, G. Zhao, L. Xu, J. M. Ward, L. Yang, and S. Nic Chormaic, Opt. Lett. **41**, 5266 (2016).
[6] X. Shen, R. C. Beltran, V. M. Diep, S. Soltani, and A. M. Armani, Sci. Adv. **4**, eaao4507 (2018).
[7] K. Tian, J. Yu, F. Lei, J. Ward, A. Li, P. Wang, and S. Nic Chormaic, Photon. Res. **10**, 2073 (2022).
[8] A. Dutt, K. Luke, S. Manipatruni, A. L. Gaeta, P. Nussenzveig, and M. Lipson, Phys. Rev. Appl. **3**, 044005 (2015).
[9] Y. K. Chembo, Phys. Rev. A **93**, 033820 (2016).
[10] M. Kues, C. Reimer, P. Roztocki, L. R. Cortés, S. Sciara, B. Wetzel, Y. Zhang, A. Cino, S. T. Chu, B. E. Little *et al.*, Nature (London) **546**, 622 (2017).
[11] P. Imany, J. A. Jaramillo-Villegas, O. D. Odele, K. Han, D. E. Leaird, J. M. Lukens, P. Lougovski, M. Qi, and A. M. Weiner, Opt. Express **26**, 1825 (2018).
[12] A. B. Matsko, Phys. Rev. A **99**, 023843 (2019).
[13] X. Lu, Q. Li, D. A. Westly, G. Moille, A. Singh, V. Anant, and K. Srinivasan, Nat. Phys. **15**, 373 (2019).
[14] Y. Okawachi, M. Yu, J. K. Jang, X. Ji, Y. Zhao, B. Y. Kim, M. Lipson, and A. L. Gaeta, Nat. Commun. **11**, 4119 (2020).
[15] G. Lin, A. Coillet, and Y. K. Chembo, Adv. Opt. Photonics **9**, 828 (2017).
[16] Y. Li, X. Jiang, G. Zhao, and L. Yang, arXiv:1809.04878.
[17] J. S. Levy, A. Gondarenko, M. A. Foster, A. C. Turner-Foster, A. L. Gaeta, and M. Lipson, Nat. Photonics **4**, 37 (2010).
[18] L. Razzari, D. Duchesne, M. Ferrera, R. Morandotti, S. Chu, B. Little, and D. Moss, Nat. Photonics **4**, 41 (2010).
[19] B. Hausmann, I. Bulu, V. Venkataraman, P. Deotare, and M. Lončar, Nat. Photonics **8**, 369 (2014).
[20] M. Pu, L. Ottaviano, E. Semenova, and K. Yvind, Optica **3**, 823 (2016).
[21] Q. Li, M. Davanço, and K. Srinivasan, Nat. Photonics **10**, 406 (2016).
[22] X. Ji, F. A. Barbosa, S. P. Roberts, A. Dutt, J. Cardenas, Y. Okawachi, A. Bryant, A. L. Gaeta, and M. Lipson, Optica **4**, 619 (2017).
[23] Y. Tang, Z. Gong, X. Liu, and H. X. Tang, Opt. Lett. **45**, 1124 (2020).
[24] C. Wang, Z. Fang, A. Yi, B. Yang, Z. Wang, L. Zhou, C. Shen, Y. Zhu, Y. Zhou, R. Bao *et al.*, Light Sci. Appl. **10**, 139 (2021).
[25] G. Marty, S. Combrié, F. Raineri, and A. De Rossi, Nat. Photonics **15**, 53 (2021).
[26] N. L. B. Sayson, T. Bi, V. Ng, H. Pham, L. S. Trainor, H. G. Schwefel, S. Coen, M. Erkintalo, and S. G. Murdoch, Nat. Photonics **13**, 701 (2019).
[27] S. Fujii, S. Tanaka, M. Fuchida, H. Amano, Y. Hayama, R. Suzuki, Y. Kakinuma, and T. Tanabe, Opt. Lett. **44**, 3146 (2019).
[28] X. Lu, G. Moille, A. Singh, Q. Li, D. A. Westly, A. Rao, S.-P. Yu, T. C. Briles, S. B. Papp, and K. Srinivasan, Optica **6**, 1535 (2019).
[29] X. Lu, G. Moille, A. Rao, D. A. Westly, and K. Srinivasan, Optica **7**, 1417 (2020).
[30] R. R. Domeneguetti, Y. Zhao, X. Ji, M. Martinelli, M. Lipson, A. L. Gaeta, and P. Nussenzveig, Optica **8**, 316 (2021).
[31] J. R. Stone, G. Moille, X. Lu, and K. Srinivasan, Phys. Rev. Appl. **17**, 024038 (2022).
[32] S. Radic, Laser Photonics Rev. **2**, 498 (2008).
[33] Z. Ye, P. Zhao, K. Twayana, M. Karlsson, V. Torres-Company, and P. A. Andrekson, Sci. Adv. **7**, eabi8150 (2021).
[34] T. Herr, K. Hartinger, J. Riemensberger, C. Wang, E. Gavartin, R. Holzwarth, M. Gorodetsky, and T. Kippenberg, Nat. Photonics **6**, 480 (2012).
[35] V. Torres-Company, D. Castelló-Lurbe, and E. Silvestre, Opt. Express **22**, 4678 (2014).
[36] B. P.-P. Kuo, J. M. Fini, L. Grüner-Nielsen, and S. Radic, Opt. Express **20**, 18611 (2012).
[37] C. M. Gentry, X. Zeng, and M. A. Popović, Opt. Lett. **39**, 5689 (2014).
[38] X. Lu, A. McClung, and K. Srinivasan, Nat. Photonics **16**, 66 (2022).
[39] D. T. Spencer, J. F. Bauters, M. J. Heck, and J. E. Bowers, Optica **1**, 153 (2014).
[40] M. H. P. Pfeiffer, J. Liu, M. Geiselmann, and T. J. Kippenberg, Phys. Rev. Appl. **7**, 024026 (2017).
[41] C. W. Hsu, B. Zhen, A. D. Stone, J. D. Joannopoulos, and M. Soljačić, Nat. Rev. Mater. **1**, 16048 (2016).

[42] S. I. Azzam and A. V. Kildishev, Adv. Opt. Mater. **9**, 2001469 (2021).
[43] T. Lepetit, E. Akmansoy, J.-P. Ganne, and J.-M. Lourtioz, Phys. Rev. B **82**, 195307 (2010).
[44] C. M. Gentry and M. A. Popović, Opt. Lett. **39**, 4136 (2014).
[45] C.-L. Zou, J.-M. Cui, F.-W. Sun, X. Xiong, X.-B. Zou, Z.-F. Han, and G.-C. Guo, Laser Photonics Rev. **9**, 114 (2015).
[46] M. V. Rybin, K. L. Koshelev, Z. F. Sadrieva, K. B. Samusev, A. A. Bogdanov, M. F. Limonov, and Y. S. Kivshar, Phys. Rev. Lett. **119**, 243901 (2017).
[47] E. A. Bezus, D. A. Bykov, and L. L. Doskolovich, Photon. Res. **6**, 1084 (2018).
[48] Z. Yu, X. Xi, J. Ma, H. K. Tsang, C.-L. Zou, and X. Sun, Optica **6**, 1342 (2019).
[49] H. Hodaei, A. Hassan, W. Hayenga, M. Miri, D. Christodoulides, and M. Khajavikhan, Opt. Lett. **41**, 3049 (2016).
[50] A. Kodigala, T. Lepetit, Q. Gu, B. Bahari, Y. Fainman, and B. Kanté, Nature (London) **541**, 196 (2017).
[51] C. Huang, C. Zhang, S. Xiao, Y. Wang, Y. Fan, Y. Liu, N. Zhang, G. Qu, H. Ji, J. Han *et al.*, Science **367**, 1018 (2020).
[52] A. A. Yanik, A. E. Cetin, M. Huang, A. Artar, S. H. Mousavi, A. Khanikaev, J. H. Connor, G. Shvets, and H. Altug, Proc. Natl. Acad. Sci. U.S.A. **108**, 11784 (2011).
[53] B. Zhen, S.-L. Chua, J. Lee, A. W. Rodriguez, X. Liang, S. G. Johnson, J. D. Joannopoulos, M. Soljačić, and O. Shapira, Proc. Natl. Acad. Sci. U.S.A. **110**, 13711 (2013).
[54] L. Carletti, K. Koshelev, C. De Angelis, and Y. Kivshar, Phys. Rev. Lett. **121**, 033903 (2018).
[55] K. Koshelev, S. Kruk, E. Melik-Gaykazyan, J.-H. Choi, A. Bogdanov, H.-G. Park, and Y. Kivshar, Science **367**, 288 (2020).
[56] V. A. Zakharov and A. N. Poddubny, Phys. Rev. A **101**, 043848 (2020).
[57] Z. Liu, Y. Xu, Y. Lin, J. Xiang, T. Feng, Q. Cao, J. Li, S. Lan, and J. Liu, Phys. Rev. Lett. **123**, 253901 (2019).
[58] S. D. Krasikov, A. A. Bogdanov, and I. V. Iorsh, Phys. Rev. B **97**, 224309 (2018).
[59] T. Wang, Z. Li, and X. Zhang, Photon. Res. **5**, 629 (2017).
[60] H. Friedrich and D. Wintgen, Phys. Rev. A **32**, 3231 (1985).
[61] F.-M. Dittes, Phys. Rep. **339**, 215 (2000).
[62] M.-A. Miri and A. Alu, Science **363**, eaar7709 (2019).
[63] P. Peng, W. Cao, C. Shen, W. Qu, J. Wen, L. Jiang, and Y. Xiao, Nat. Phys. **12**, 1139 (2016).
[64] Y. Jiang, Y. Mei, Y. Zuo, Y. Zhai, J. Li, J. Wen, and S. Du, Phys. Rev. Lett. **123**, 193604 (2019).
[65] Y. Choi, C. Hahn, J. W. Yoon, and S. H. Song, Nat. Commun. **9**, 2182 (2018).
[66] Y. Yang, Y.-P. Wang, J. W. Rao, Y. S. Gui, B. M. Yao, W. Lu, and C.-M. Hu, Phys. Rev. Lett. **125**, 147202 (2020).
[67] Y. Li, Y.-G. Peng, L. Han, M.-A. Miri, W. Li, M. Xiao, X.-F. Zhu, J. Zhao, A. Alù, S. Fan, and C.-W. Qiu, Science **364**, 170 (2019).
[68] F. Lei, J. M. Ward, P. Romagnoli, and S. Nic Chormaic, Phys. Rev. Lett. **124**, 103902 (2020).
[69] C. Li, D. Liu, and D. Dai, Nanophotonics **8**, 227 (2019).
[70] X. Ji, J. K. Jang, U. D. Dave, M. Corato-Zanarella, C. Joshi, A. L. Gaeta, and M. Lipson, Laser Photonics Rev. **15**, 2000353 (2021).
[71] L. Zhang, S. Hong, Y. Wang, H. Yan, Y. Xie, T. Chen, M. Zhang, Z. Yu, Y. Shi, L. Liu, and D. Dai, Laser Photonics Rev. **16**, 2100292 (2022).
[72] See Supplemental Material at http://link.aps.org/supplemental/10.1103/PhysRevLett.130.093801 for more details about theoretical model, sample characterization and H-OPO conversion efficiency analysis, which includes Refs. [73–76].
[73] C. Gardiner, P. Zoller, and P. Zoller, *Quantum Noise: A Handbook of Markovian and non-Markovian Quantum Stochastic Methods with Applications to Quantum Optics* (Springer Science & Business Media, New York, 2004).
[74] Y.-F. Xiao, M. Li, Y.-C. Liu, Y. Li, X. Sun, and Q. Gong, Phys. Rev. A **82**, 065804 (2010).
[75] Z. Ye, K. Twayana, P. A. Andrekson, and V. Torres-Company, Opt. Express **27**, 35719 (2019).
[76] K. Twayana, Z. Ye, Ó. B. Helgason, K. Vijayan, M. K, and V. Torres-Company, Opt. Express **29**, 24363 (2021).
[77] Y. Zhang, M. Menotti, K. Tan, V. Vaidya, D. Mahler, L. Helt, L. Zatti, M. Liscidini, B. Morrison, and Z. Vernon, Nat. Commun. **12**, 2233 (2021).
[78] Y. Zhao, Y. Okawachi, J. K. Jang, X. Ji, M. Lipson, and A. L. Gaeta, Phys. Rev. Lett. **124**, 193601 (2020).
[79] Z. Yang, M. Jahanbozorgi, D. Jeong, S. Sun, O. Pfister, H. Lee, and X. Yi, Nat. Commun. **12**, 4781 (2021).
[80] F. A. Sabattoli, H. El Dirani, L. Youssef, F. Garrisi, D. Grassani, L. Zatti, C. Petit-Etienne, E. Pargon, J. E. Sipe, M. Liscidini, C. Sciancalepore, D. Bajoni, and M. Galli, Phys. Rev. Lett. **127**, 033901 (2021).
[81] F. Lei, Z. Ye, K. Twayana, Y. Gao, M. Girardi, O. B. Helgason, P. Zhao, and V. Torres-Company, [year], [version number], Zenodo (2023), version 1, 10.5281/zenodo.7529404.